

## EDGE ARTICLE

Cite this: *Chem. Sci.*, 2024, 15, 5596

† All publication charges for this article have been paid for by the Royal Society of Chemistry

Structure and photochemistry of di-*tert*-butyldiphosphatetrahedrane†‡

Gabriele Hierlmeier,<sup>§\*</sup> Roger Jan Kutta,<sup>||<sup>b</sup></sup> Peter Coburger,<sup>||<sup>a</sup></sup> Hans-Georg Stammler,<sup>||<sup>c</sup></sup> Jan Schwabedissen,<sup>c</sup> Norbert W. Mitzel,<sup>||<sup>\*c</sup></sup> Maria Dimitrova,<sup>||<sup>de</sup></sup> Raphael J. F. Berger,<sup>||<sup>e</sup></sup> Patrick Nuernberger<sup>||<sup>\*b</sup></sup> and Robert Wolf<sup>||<sup>\*a</sup></sup>

Di-*tert*-butyldiphosphatetrahedrane (*t*BuCP)<sub>2</sub> (**1**) is a mixed carbon- and phosphorus-based tetrahedral molecule, isolobal to white phosphorus (P<sub>4</sub>). However, despite the fundamental significance and well-explored reactivity of the latter molecule, the precise structure of the free (*t*BuCP)<sub>2</sub> molecule (**1**) and a detailed analysis of its electronic properties have remained elusive. Here, single-crystal X-ray structure determination of **1** at low temperature confirms the tetrahedral structure. Furthermore, quantum chemical calculations confirm that **1** is isolobal to P<sub>4</sub> and shows a strong largely isotropic diamagnetic response in the magnetic field and thus pronounced spherical aromaticity. A spectroscopic and computational study on the photochemical reactivity reveals that diphosphatetrahedrane **1** readily dimerises to the ladderane-type phosphaaalkyne tetramer (*t*BuCP)<sub>4</sub> (**2**) under irradiation with UV light. With sufficient thermal activation energy, the dimerisation proceeds also in the dark. In both cases, an isomerisation to a 1,2-diphosphacyclobutadiene **1'** is the first step. This intermediate subsequently undergoes a [2 + 2] cycloaddition with a second 1,2-diphosphacyclobutadiene molecule to form **2**. The 1,2-diphosphacyclobutadiene intermediate **1'** can be trapped chemically by *N*-methylmaleimide as an alternative [2 + 2] cycloaddition partner.

Received 8th February 2024

Accepted 8th March 2024

DOI: 10.1039/d4sc00936c

rsc.li/chemical-science

## Introduction

The tetrahedron is a fundamental structure motif in chemistry. Tetrahedral molecules can incorporate various elements of the periodic table, including s-, p- and d-block elements. Among the most prominent examples are the first “organic” tetrahedrane, (*t*BuC)<sub>4</sub>,<sup>1</sup> and the prototype of “inorganic” tetrahedrane, P<sub>4</sub>.<sup>2,3</sup>

<sup>a</sup>Universität Regensburg, Institut für Anorganische Chemie, 93040 Regensburg, Germany. E-mail: robert.wolf@ur.de

<sup>b</sup>Universität Regensburg, Institut für Physikalische und Theoretische Chemie, 93040 Regensburg, Germany. E-mail: Patrick.Nuernberger@chemie.uni-regensburg.de

<sup>c</sup>Universität Bielefeld, Lehrstuhl für Anorganische Chemie und Strukturchemie, Universitätsstraße 25, 33615 Bielefeld, Germany. E-mail: nmitzel@uni-bielefeld.de

<sup>d</sup>Department of Chemistry, University of Helsinki, Faculty of Science, FI-00014 Helsinki, Finland

<sup>e</sup>Paris Lodron Universität Salzburg, Chemie und Physik der Materialien, 5020 Salzburg, Austria

† We dedicate this manuscript to the memory of Manfred Regitz.

‡ Electronic supplementary information (ESI) available. CCDC 2102564–2323059. For ESI and crystallographic data in CIF or other electronic format see DOI: <https://doi.org/10.1039/d4sc00936c>

§ Present address: Julius-Maximilians-Universität Würzburg, Institut für Anorganische Chemie, Am Hubland, 97074 Würzburg.

¶ Present address: Technische Universität München, Lehrstuhl für Anorganische Chemie mit Schwerpunkt neue Materialien, Lichtenbergstraße 4, 85748 Garching bei München, Germany.

While the chemical properties and reactivity patterns of P<sub>4</sub> and (*t*BuC)<sub>4</sub> have been studied for a long time, the physical properties, in particular the thermal stability and photochemistry, of both molecules have also attracted considerable attention.<sup>4</sup>

The transformation of white phosphorus into its red allotrope by irradiation is well known (Fig. 1A).<sup>5</sup> It was proposed that this reaction takes place *via* photoinduced dissociation of P<sub>4</sub> into P<sub>2</sub> molecules, which then recombine to form polymeric red phosphorus.<sup>6</sup> The same equilibrium P<sub>4</sub> ⇌ P<sub>2</sub> can also be reached

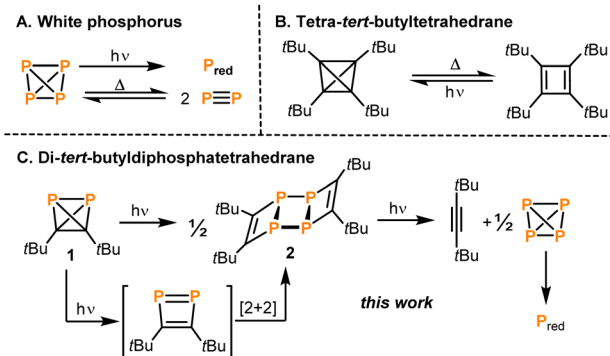


Fig. 1 Thermal and photochemical reactions of group 14/group 15 tetrahedranes.



thermally in the gas phase at temperatures above 1000 °C.<sup>7</sup> A solvent-dependent radical mechanism has also been proposed for the polymerisation of P<sub>4</sub> to red phosphorus under irradiation with ionising  $\gamma$ -rays.<sup>8</sup> The photochemistry of P<sub>4</sub> can be exploited for the synthesis of new diphosphenes *via* [2 + 4] cycloadditions of P<sub>2</sub> with dienes.<sup>9</sup>

A photochemical pathway was pursued to access the purely carbon-based tetrahedrane tetra-*tert*-butyltetrahedrane (*t*BuC)<sub>4</sub> which can be generated by irradiation of its cyclobutadiene isomer tetra-*tert*-butylcyclobutadiene ( $\lambda > 300$  nm; Fig. 1B).<sup>1</sup> Above 130 °C, (*t*BuC)<sub>4</sub> undergoes back-isomerisation to the tetra-*tert*-butylcyclobutadiene.

Recently, the synthesis and reactivity of di-*tert*-butyldiphosphatetrahedrane (**1**), the “hybrid” of P<sub>4</sub> and (*t*BuC)<sub>4</sub>,<sup>3,10,11</sup> as well as the related tri-*tert*-butylphosphatetrahedrane (*t*Bu<sub>3</sub>C<sub>3</sub>P)<sup>12</sup> and triphosphatetrahedrane (HCP<sub>3</sub>)<sup>12</sup> have been described. Diphosphatetrahedrane **1** is readily prepared by a nickel-catalysed dimerisation reaction of *tert*-butylphosphaalkyne *t*BuCP and is isolated as a metastable liquid with a melting point of –32 °C. Above its melting point, **1** slowly dimerises to give the known ladderane-type phosphalkyne tetramer (*t*BuCP)<sub>4</sub> (**2**).<sup>13</sup> As a result, attempts to grow single crystals of **1** by standard techniques were unsuccessful previously, while the structure of the silver(i) complex [( $\eta^2$ -**1**)Ag(2)]<sub>2</sub>[Al(OR<sup>F</sup>)<sub>4</sub>] [**1-Ag**, R<sup>F</sup> = C(CF<sub>3</sub>)<sub>3</sub>] could be determined. **1-Ag** shows an intact P<sub>2</sub>C<sub>2</sub> tetrahedron side-on coordinated to an Ag<sup>+</sup> cation.

Here, the structure of **1** in the solid state by single-crystal X-ray diffraction is determined and, according to quantum-chemical calculations, its electronic structure reveals a pronounced spherical aromaticity comparable to that in P<sub>4</sub> and (*t*BuC)<sub>4</sub>. Furthermore, the temperature and light sensitivity of **1** is presented in more detail and the remarkable photochemistry of **1** is reported. Irradiation of **1** with UV light affords **2** *via* [2 + 2] cycloaddition of two intermediate 1,2-diphosphacyclobutadienes (Fig. 1C). The photochemistry of **1** reveals notable differences in comparison with the photochemistry of P<sub>4</sub>, (*t*BuCP)<sub>4</sub> and *t*BuCP (the monomer of **1**). Moreover, the present study complements recent results on the related tri-*tert*-butylphosphatetrahedrane (*t*Bu<sub>3</sub>C<sub>3</sub>P), which was shown by Cummins and co-workers to isomerise to a planar phosphacyclobutadiene upon addition of the Lewis acid BPh<sub>3</sub>.<sup>14</sup>

## Results and discussion

### X-ray crystallography

Crystallographic structure determination of the title compound **1** by X-ray-diffraction (XRD) was challenging because **1** is a liquid at ambient temperature, which is simultaneously sensitive to air, light and temperature. Numerous attempts to grow a single crystal from the liquid phase were unsuccessful, because the decomposition of **1** started immediately after melting, producing crystal seeds that led to polycrystalline specimens. Moreover, the crystallisation process is difficult to monitor and control, because the observation with polarised light also leads to decomposition. In one of the crystallisation experiments, a crystalline region in the capillary was observed, which turned out to be di-*tert*-butylacetylene (the structure of which had already been determined earlier).<sup>15</sup>

To overcome these problems, mixing **1** with *n*-pentane lowered the melting point, allowing crystal growth at a lower temperature, where the sample is sufficiently stable for the time needed to grow a crystalline sample. For this, a freshly prepared mixture of **1** and *n*-pentane was transferred to a capillary and using the cryo-stream of the diffractometer immediately cooled in the dark from 240 K with 5 K h<sup>–1</sup> to 180 K and subsequently to 94 K with a max. cooling rate. A colourless crystal was obtained, which was twinned with ratio of 1:1. The second domain was rotated by –169.1° around [010] (reciprocal). Both domains were taken into account for data integration and only the non- or minor-overlapping reflections of the first domain were used for refinement. **1** crystallised in the monoclinic space group *P*2<sub>1</sub> with one molecule per asymmetric unit (Fig. 2). Important bond lengths are summarised in Table 1 and compared with those calculated by coupled cluster theory or found in the molecular structure of the silver(i) complex **1-Ag** (Fig. 3 and Table 1).

The P1–P2 bond length of 2.205(1) Å in **1** compares well to the bond length in P<sub>4</sub> determined by gas phase electron diffraction ( $r_g = 2.1994(3)$  Å).<sup>2</sup> Moreover, the P–C bond lengths range from 1.845(2) to 1.849(2) Å and the C1–C2 bond length of 1.458(2) Å is very similar to that found in (*t*BuC)<sub>4</sub> (average: 1.485 Å).<sup>16</sup>

Overall, the bond lengths compare very well to the calculations at the DLPNO-CCSD(T)/def2-QZVPP level of theory (Table 1). Moreover, comparison of the bond metrics with the previously reported Ag(i) complex **1-Ag** reveals the expected extension of the P–P bond by *ca.* 0.1 Å to 2.308(3) Å upon coordination. The differences in C1–C2 and P–C bond lengths were less pronounced.

It should be noted that despite numerous attempts to determine the structure of **1** by gas electron diffraction, suitable conditions could not be found to record consistent diffraction patterns.

### Electronic structure

Previously, an analogy in the reactivity of **1** and P<sub>4</sub> had been noticed, which may be attributed to the isolobal analogy. In this concept, the frontier orbitals of two molecules are compared with respect to their energies, shape, occupation and symmetry.<sup>17</sup>

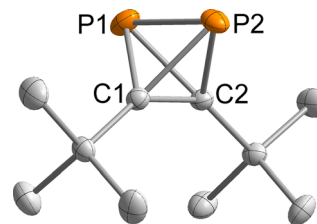
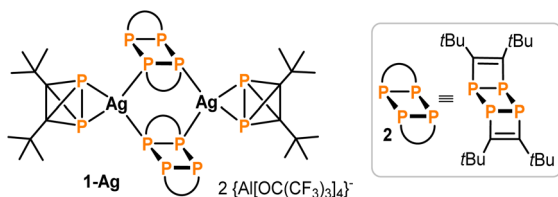


Fig. 2 Molecular structure of **1** in the solid state. Thermal ellipsoids are set at the 50% probability level. Hydrogen atoms are omitted for clarity. Selected bond lengths [Å] and angles [°]: P1–P2 2.205(1), P1–C1 1.845(2), P1–C2 1.847(2), P2–C1 1.849(2), P2–C2 1.846(2), C1–C2 1.458(2), C1–P1–P2 53.4(1), C2–P1–P2 53.3(1), C2–P1–C1 46.5(1), C1–P2–P1 53.3(1), C1–P2–C2 46.5(1), C2–P2–P1 53.3(1), P2–C1–P1 73.3(1), C2–C1–P1 66.8(1), C2–C1–P2 66.7(1), P1–C2–P2 73.3(1), C1–C2–P1 66.7(1), C1–C2–P2 66.9(1).

**Table 1** Comparison of bond lengths in solid state structures of **1** with calculated values obtained using DLPNO CCSD(T)/def2-QZVPP of the single molecule<sup>10</sup>

| Bond  | Bond length [Å] XRD ( <b>1</b> ) | Bond length [Å] DLPNO CCSD(T) ( <b>1</b> ) | Bond length [Å] XRD ( <b>1-Ag</b> ) |
|-------|----------------------------------|--|-------------------------------------|
| P1–P2 | 2.205(1)                         | 2.203                                      | 2.308(3)                            |
| C1–C2 | 1.458(2)                         | 1.458                                      | 1.462(12)                           |
| P–C   | 1.849(2)–1.845(2)                | 1.852                                      | 1.820(8)–1.836(9)                   |



**Fig. 3** Structure of **1-Ag** (see Table 1 for selected structural data).

DFT calculations on the TPSS-D3BJ/def2-TZVP level of theory have shown that the frontier orbitals of both molecules are related in energy and shape (Fig. 4). As expected, the degeneracy of t- and e-orbitals in  $P_4$  is not preserved in **1**. The HOMO (−5.3 eV) of **1** has mainly P–C bond character, whereas the HOMO-1 (−5.7 eV) has large contributions of the P–P and C–C bonds (for a comparison of all occupied orbitals see the ESI†).

Both  $P_4$  and  $(tBuC)_4$  have been demonstrated to possess spherical aromaticity.<sup>2,18</sup> As a probe for such aromatic ring currents the nucleus independent chemical shifts (NICS) have been an effective tool in previous studies.<sup>19</sup> For comparison, the NICS values were calculated on the TPSS/pcSseg-2 level of theory

at the centre of the cages of  $P_4$ ,  $(tBuC)_4$  and **1**, affording strongly negative values of −60.1, −48.2 and −50.3 ppm, respectively. Notably, the value for  $P_4$  compares well with a recent calculation (−61.9).<sup>20,21</sup> The value for **1** (−50.3) is in between the values for  $P_4$  and  $(tBuC)_4$ , which suggests large induced diatropic ring currents. A calculation of the magnetically induced total ring current flux in  $P_4$ , **1** and  $(tBuC)_4$  yielded 24, 15 (and 16 in one orthogonal direction) and 16 nA T<sup>−1</sup>, respectively (Fig. 5, B3LYP/def2-TZVP; see the ESI† for details).<sup>22</sup> The strong diamagnetic response of  $P_4$  underlines its aromatic nature, while the directional independence (isotropy) of the flux in **1** suggests the presence of spherical aromaticity (as it is already imposed by symmetry upon  $P_4$  and  $(tBuC)_4$ ). Moreover, the high flux values demonstrate a significant amount of aromatic cluster current in **1** and  $(tBuC)_4$  (for comparison, benzene shows a total ring current of approx. 12 nA T<sup>−1</sup>).<sup>23</sup>

### Photochemistry

As evidenced by monitoring the characteristic <sup>31</sup>P NMR signal at −468.2 ppm (see Fig. S21, ESI†) the concentration of **1** stays constant over 15 hours in the dark at ambient temperature in

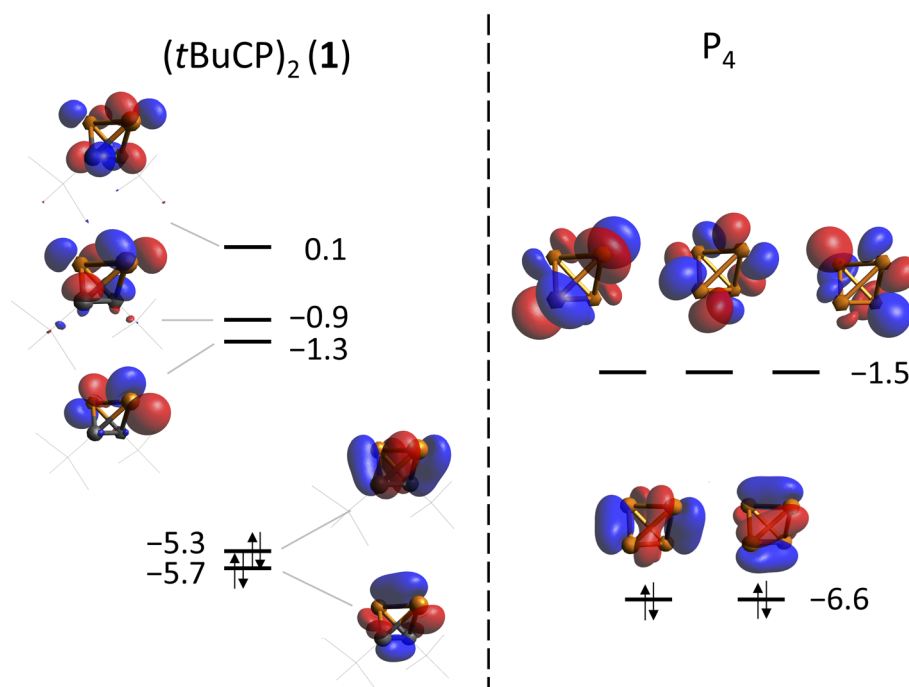


**Fig. 4** Frontier orbitals of **1** (left) and  $P_4$  (right) calculated at the TPSS-D3BJ/def2-TZVP level of theory. Energies are given in eV.

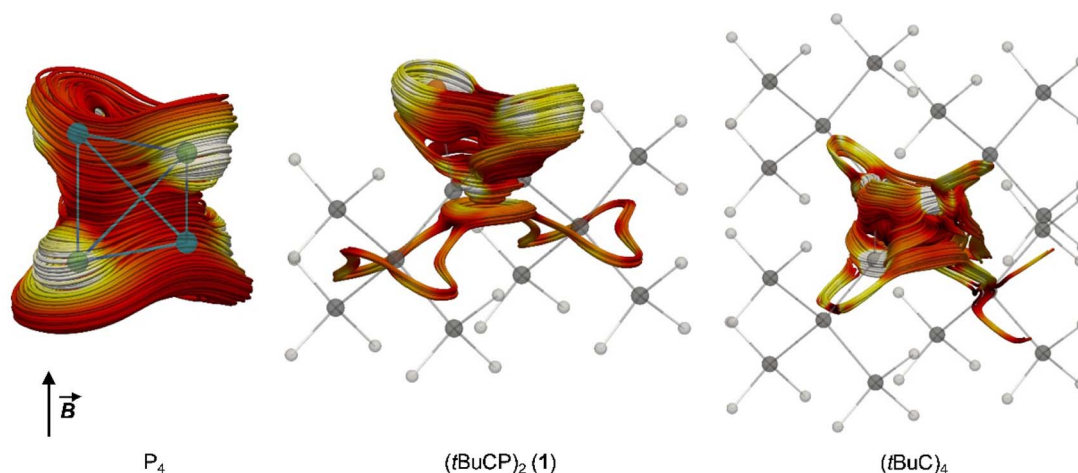


Fig. 5 Spaghetti plots of selected current density streamlines induced by an external magnetic field ( $B$ ) showing the main cluster current contributions for  $P_4$ , **1** and  $(tBuC)_4$ , respectively. For details on the calculations, see the ESI.†

solution. However, at temperatures above 40 °C, the formation of the ladderane  $(tBuCP)_4$  (**2**) (*i.e.* a dimer of **1**, see Fig. 1) was observed by a singlet resonance at  $-22.2$  ppm (Fig. S19 in the ESI.†).<sup>13</sup> Correspondingly, conversion of **1** to **2** increases with higher temperatures. For instance, keeping the solution at 80 °C for *ca.* 2.5 hours results in *ca.* 8% conversion (based on integration) of **1** to **2** (Fig. S21.†). This thermal instability of **1** is in agreement with a previous report.<sup>10</sup>

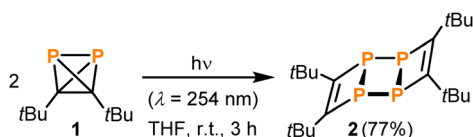
Upon exposure to ambient light, **1** showed a significantly lower stability as demonstrated by preparing two identical samples containing **1** (with a concentration of  $0.44 \text{ mol L}^{-1}$ ) and an internal standard ( $PPh_3$ ) in  $C_6D_6$  and monitoring the corresponding characteristic  $^{31}P$  NMR signals quantitatively in the dark and in the light, respectively (Fig. S9 and S10.†). While the sample kept in the dark did not degrade notably over time, the sample kept under ambient light was partly converted into **2** after 17 hours. Note that the conversion was not complete with a final concentration of  $0.04 \text{ mol L}^{-1}$  (corresponding to 90% conversion) for **1** and  $0.15 \text{ mol L}^{-1}$  (corresponding to 68% yield) for **2**, which is presumably explained by the formation of a precipitate in the NMR tube (*vide infra*).

The photochemical instability of **1** allowed the development of a convenient protocol for the synthesis of **2** from **1**. Irradiation of solutions of **1** in THF for three hours using a UV lamp and subsequent extraction with benzene results in pure **2** in 77% isolated yield (Scheme 1). No side products were detected when following the reaction by  $^{31}P$  NMR spectroscopy.

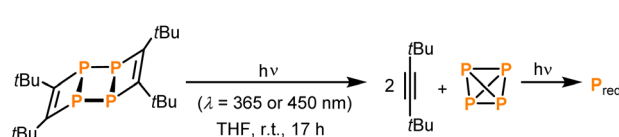
It is important to note that tri-*tert*-butylphosphatetrahedrane ( $tBu_3C_3P$ ) undergoes a very similar reaction with substoichiometric amounts of a Lewis acid such as

triphenylborane, affording a planar phosphacyclobutadiene.<sup>14</sup> In the absence of other reagents, this species undergoes head-to-head dimerisation to form a ladderane-type dimer similar to **2**. In the presence of alkenes or a transition metal complex, however, it could be trapped as cycloaddition product or as a ligand. The photochemistry (when exciting at 254 nm) of  $(tBu_3C_3P)$  is rather unselective, affording a mixture of products including the dicyclopropenyl substituted diphosphene. In contrast, the dimerisation of **1** to **2** is driven photochemically and does not require the addition of further reagents.

Under prolonged irradiation of **2** in THF with either 365 nm or 450 nm a reaction mixture consisting of an orange precipitate and a colourless solution is obtained (see Fig. S5 in the ESI.†). Analysis of the solution by  $^1H$  NMR spectroscopy revealed clean conversion to di-*tert*-butylacetylene as evidenced by a singlet resonance at a chemical shift of 1.34 ppm and the absence of starting material (see Fig. S15 in the ESI.† as described above, this formation of di-*tert*-butylacetylene was already observed in attempts to crystallise pure **1** *in situ* on the diffractometer). The  $^{13}C\{^1H\}$  NMR spectrum also showed the three signals corresponding to the alkyne at chemical shifts of 27.4, 31.7 and 87.5 ppm (Fig. S16.†). The  $^{31}P\{^1H\}$  NMR spectrum showed a small amount of  $P_4$  at  $-520.7$  ppm (see Fig. S17 in the ESI.†). Thus, the orange precipitate is assigned to red phosphorus (or a related phosphorus containing polymer), which has been observed to form upon polymerisation of white phosphorus in other reactions induced by ionising  $\gamma$ -radiation (Scheme 2).<sup>8</sup> Notably, this is reminiscent of the reactivity of tetrahedral  $Co_2(CO)_6(\eta^2\text{-alkyne})$  complexes, where the  $Co_2(CO)_6$  can act as protecting group.<sup>24</sup>



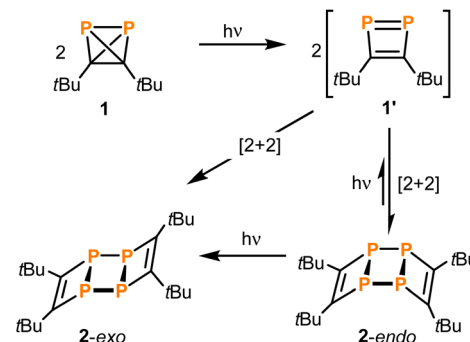
Scheme 1 Synthesis of **2** by irradiating **1**.



Scheme 2 Photochemistry of **2**.

At significantly lower concentrations of **1**, the photo-conversion of **1** to **2** proceeds *via* a further intermediate, which can be monitored as a complete step prior to further degradation, as evidenced by recording the electronic absorption spectra in the UV/vis after stepwise illumination at 340 nm of a 500  $\mu\text{M}$  solution of **1** in *n*-hexane (Fig. 6). Within the first 5 s of illumination, the absorption spectrum of **1** with two characteristic bands at *ca.* 230 and 280 nm decreases while an absorption spectrum with two distinct bands peaking at *ca.* 350, 300 and 210 nm is formed. On prolonged illumination the formed absorption spectrum becomes particularly more defined in the spectral range from 260 to 380 nm and resembles the absorption spectrum of purified **2** (Fig. 6).

With even longer illumination, the additional formation of elemental phosphorus and di-*tert*-butylacetylene is evidenced by scatter contributions in the UV/vis absorption signal (data not shown). Based on the structure of **2**, it can be assumed that this ladderane compound is formed by cycloaddition of two P=P bonds of two planar 1,2-diphosphacyclobutadienes **1'** (Scheme 3).<sup>25</sup> To investigate this possibility, molecular dynamics simulations of **1** were performed starting in the electronic ground state and switching into the first excited singlet state after 1 ps of propagation. These simulations provide striking evidence for a formation of planar 1,2-diphosphacyclobutadienes upon illumination (Fig. 7 and S24 and ESI



Scheme 3 Proposed mechanism for the dimerisation of **1** to **2**.

movie†). Directly after changing to the first excited singlet state the P–P bond length increases instantaneously (Fig. 7a). Within a time-window of 2 ps of propagation, the molecular framework flips into a rather planar trapezoid shape (**1'**). Notably, the formation of **1'** from **1** in the absence of light has a computed activation barrier of 55.3 kcal mol<sup>-1</sup> according to DFT calculations on the  $\omega\text{B97X-D3/def2-SVP}$  level of theory using the NEB method.

Dimerisation of **1'** should generally be allowed to form either the *endo*- or *exo*-configured ladderane **2**. In both cases no noticeable activation barrier is expected (Fig. 8). Since the observed intermediate shows a spectrum rather similar to the final spectrum of **2** and the fact that the *exo*-isomer is more stable by 0.5 eV (12 kcal mol<sup>-1</sup>), it is tempting to speculate that the intermediate represents the *endo*-form of **2**, which can be photochemically converted into the more stable *exo*-form.<sup>26</sup> The

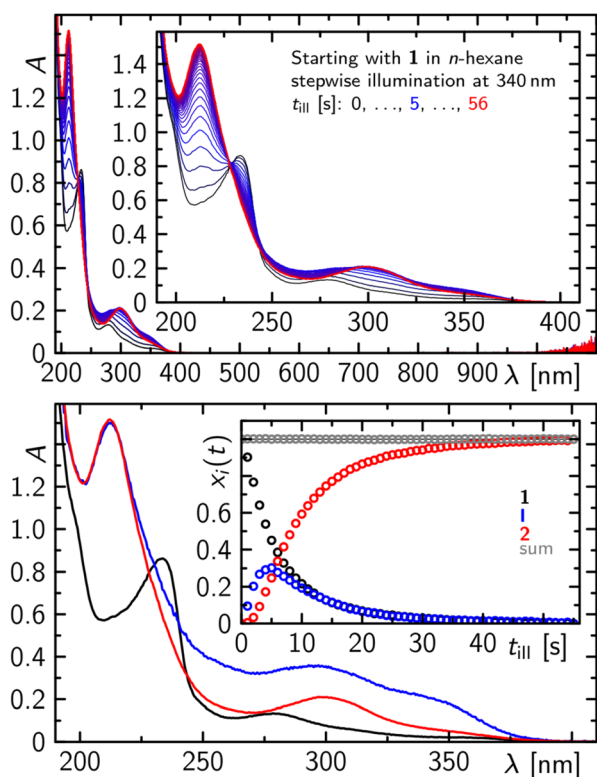


Fig. 6 Sequence of absorption spectra of **1** (2 mM) in *n*-hexane after stepwise illumination at 340 nm with rectangular pulses of 1 s pulse width (top) and the corresponding decomposition into species spectra and concentration time profiles showing clearly an intermediate **1** prior to the final formation of **2** (bottom).

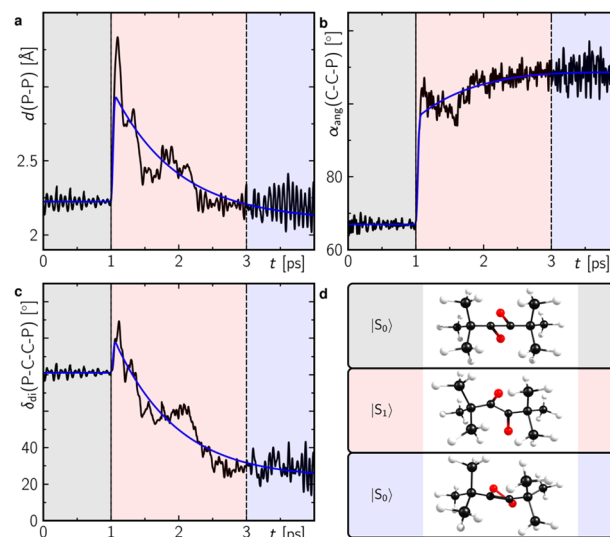


Fig. 7 Structural analysis of the molecular dynamics trajectories showing the average of the P–P bond length (a), the carbon–carbon–phosphorus angle (b) and the P–C–C–P dihedral angle (c) as defined in (d) of Fig. S24.† The colour shaded temporal ranges indicate propagation in different electronic state as indicated in (d). Corresponding representative structures during this temporal range are also shown in (d). The blue lines in (a–c) correspond to a global monoexponential fit to the data with a lifetime of *ca.* 960 fs.

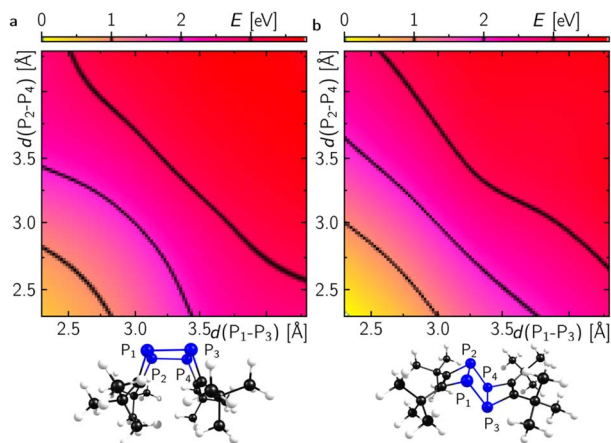
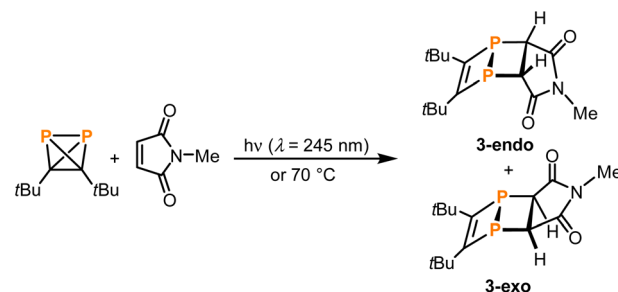


Fig. 8 Potential energy surfaces along the dimerisation coordinates of two molecules of **1** to **2** in either the *endo*- (a) or the *exo*-configuration (b). Calculations were performed at the B3LYP-D4/def2-TZVP level of theory.

calculated absorption spectrum of the *exo*-configured isomer shows a rather defined absorption band peaking at *ca.* 300 nm with a shoulder at around 350 nm as observed in the experiment for the final product **2-exo**. Importantly, the calculated spectrum of the *endo*-isomer shows a higher absorptivity red and blue shifted compared to the main absorption band of the *exo*-isomer peaking at *ca.* 270 and 350 nm, respectively, which is also observed in the experiment. This provides evidence for the assignment of a photoinduced *endo* to *exo* isomerisation of **2**. Alternatively, a photoinduced retro-[2 + 2] cycloaddition from **2-endo** to **1**' and subsequent [2 + 2] to **2-exo** could take place.<sup>27</sup>

Next, reactions of **1** with suitable trapping agents for [2 + 2] cycloadditions, *i.e.*, alkenes or alkynes, were tested as experimental indications for the occurrence of a 1,2-diphosphacyclobutadiene as an intermediate in the formation of **2** from **1**. While irradiating **1** at 254 nm in the presence of either bis-(trimethylsilyl)acetylene or maleic anhydride resulted only in the formation of **2** as observed for **1** alone,<sup>28</sup> the reaction of **1** with the more electron-deficient *N*-phenylmaleimide gave two singlet resonances ( $\delta = -63.0$  and  $-84.4$  ppm) in the  $^{31}\text{P}\{^1\text{H}\}$  NMR spectrum after irradiation for two hours (see Fig. S18 in the ESI†). This reaction was more selective (affording less **2**) when excess amounts of the alkene were employed. However, from a synthetic point of view, the removal of this excess proved difficult due to similar solubilities and retention factors during chromatographic separation. Therefore, the smaller *N*-methylmaleimide was chosen for the trapping reaction. The  $^{31}\text{P}\{^1\text{H}\}$  NMR spectrum of the product showed two distinct signals at chemical shifts of  $-62.4$  and  $-84.6$  ppm. Removal of the excess *N*-methylmaleimide by sublimation and recrystallisation of the residue from *n*-hexane afforded single crystals of both of the isomeric [2 + 2] cycloaddition products **3-endo** and **3-exo** (Scheme 4).

Single-crystal XRD diffraction revealed that **3-exo** and **3-endo** co-crystallise in the space group  $P2_1/c$  with eight molecules of **3-exo** and four molecules **3-endo** in the unit cell. The molecular structures of **3-exo** and **3-endo** in the solid state (Fig. 9) strongly



Scheme 4 [2 + 2]-Cycloadditions of *in situ* generated 1,2-diphosphacyclobutadiene **1'** with *N*-methylmaleimide.

support the formation of diphosphabicyclo[2.2.0]hexene rings formed upon [2 + 2] cycloaddition of an *in situ* generated 1,2-diphosphacyclobutadiene with *N*-methylmaleimide. This is consistent with the proposed mechanism for the dimerisation of **1** to **2** via a 1,2-diphosphacyclobutadiene. In both **3-exo** and **3-endo**, the P–P bond lengths [P1–P2 2.242(1) Å, P5–P6 2.233(1) Å] are indicative of a single bond and the C–C bonds originating from **1** have bond lengths typical for double bonds [C1–C2 1.362(3) Å, C32–C31 1.367(3) Å].<sup>29</sup> The C–C bonds originating from the maleimide possess typical bond lengths for single bonds [C11–C12 1.524(2) Å, C41–C42 1.523(2) Å]. The C2–P2–C12 and C1–P1–C11 angles of 97.8(1)° and 95.5(1)°, respectively, indicate an almost perpendicular arrangement of the two C<sub>2</sub>P<sub>2</sub> rings in **3-exo**. In **3-endo**, these angles are larger [C31–P5–C41: 100.8(1)°, C32–P6–C42: 100.7(1)°] possibly resulting from steric hindrance of the *tert*-butyl groups and the imide moiety.

According to the  $^1\text{H}$  and  $^{31}\text{P}\{^1\text{H}\}$  (single and multinuclear) NMR spectra as well as mass spectra, **3-exo** and **3-endo** were isolated as a mixture containing *ca.* 53% of the *endo*- and 47% of

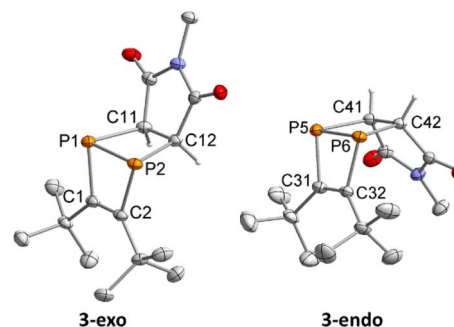


Fig. 9 Molecular structures of **3-endo** and **3-exo** in the solid state. Thermal ellipsoids are set at 50% probability level. H-atoms (except for those binding to C11, C12, C41 and C42) are omitted for clarity. Selected bond lengths [Å] and angles [°]: P1–P2 2.242(1), P1–C1 1.844(2), P1–C11 1.916(2), P2–C2 1.852(2), P2–C12 1.910(2), C1–C2 1.362(3), C11–C12 1.524(2), P5–P6 2.233(1), P5–C31 1.841(2), P5–C41 1.928(2), P6–C32 1.841(2), P6–C42 1.923(2), C32–C31 1.367(3), C41–C42 1.523(2), C1–P1–P2 76.4(1), C2–P2–P1 75.9(1), C1–C2–P2 103.8(1), C2–C1–P1 103.7(1), C11–P1–P2 79.5(1), C12–P2–P1 78.7(1), C12–C11–P1 100.0(1), C11–C12–P2 101.5(1), C2–P2–C12 97.8(1), C1–P1–C11 95.5(1), C31–P5–P6 76.2(1), C32–P6–P5 76.5(1), C32–C31–P5 103.8(1), C31–C32–P6 103.3(1), C41–P5–P6 79.1(1), C42–P6–P5 79.5(1), C41–C42–P6 100.4(1), C42–C41–P5 100.7(1), C31–P5–C41 100.8(1), C32–P6–C42 100.7(1).

the *exo*-isomer. The  $^{31}\text{P}\{^1\text{H}\}$  NMR spectrum shows two singlet signals at chemical shifts of  $-85.2$  and  $-63.1$  ppm. In the proton-coupled  $^{31}\text{P}$  NMR spectrum the signal at  $-85.2$  ppm shows coupling to the diphosphacyclobutane protons and has the shape of a pseudo-triplet, whereas the signal at  $-63.1$  ppm shows no coupling. DFT calculations at the TPSS pcSseg-2 level of theory confirm that the high-field resonance, which is assigned to **3-endo**, shows higher  $J_{\text{PH}}$  coupling constants than the low-field species. This is in agreement with the experimental values and also confirmed by a study on the effect of the lone pair conformation on P–H coupling constants.<sup>30</sup> Simulation of the  $^{31}\text{P}$  NMR signal of **3-endo** reveals a  $^2J_{\text{PH}}$  coupling constant of 13.1 Hz and a  $^3J_{\text{PH}}$  coupling constant of  $-9.7$  Hz.

The  $^1\text{H}$  NMR spectrum of the mixture of isomers **3-endo** and **3-exo** shows singlet resonances for the *tert*-butyl groups at 1.07 and 1.15 ppm and for the maleimide methyl groups at 2.65 and 2.66 ppm. Moreover, the diphosphacyclobutane proton signals arise as a singlet at 2.75 for **3-exo** and as a multiplet between 2.63 and 2.71 ppm for **3-endo**. The  $^{13}\text{C}\{^1\text{H}\}$  NMR spectrum shows two singlet resonances for the maleimide methyl groups and pseudo triplet resonances for the other carbon atoms. Four low-field-shifted resonances were assigned to the diphosphacyclobutene carbon atoms at 167.7 (**3-endo**) and 168.6 ppm (**3-exo**) and the carbonyl moieties at 175.2 (**3-endo**) and 175.9 ppm (**3-exo**). Analysis of a mixture of **3-endo** and **3-exo** by GC-MS revealed two peaks at retention times of 14.28 and 14.46 min with mass spectra that show the same, expected molecular ion signal with  $m/z = 311.0$ .

It is worth noting that a  $[2 + 2]$ -cycloaddition product related to **3-endo/exo** was synthesised by Regitz and co-workers by reacting the same maleimide with the isomeric 1,3-diphosphacyclobutadiene (generated by addition of hexachloroethane to a zirconium complex).<sup>31</sup> In Regitz's report, the formation of this isomeric diphosphabicyclo[2.2.0]hexene was confirmed by multinuclear ( $^1\text{H}$ ,  $^{13}\text{C}\{^1\text{H}\}$  and  $^{31}\text{P}\{^1\text{H}\}$ ) NMR spectroscopy and mass spectrometry. Only the *endo*-isomer was observed. Recently, also a different reaction type was reported, in which nickel complexes catalyse the phosphinidene transfer from (*t*Bu<sub>3</sub>C<sub>3</sub>P) to styrene, ethylene, neohexene and 1,3-cyclohexadiene, affording phosphiranes.<sup>14</sup>

## Conclusions

The tetrahedral molecular structure of di-*tert*-butyldiphosphate-tetrahdrane (**1**) has been unambiguously determined by single-crystal X-ray diffraction analysis at low temperature. The structure is similar to that of tetra-*tert*-butyltetrahedrane (*t*BuC)<sub>4</sub> and the P<sub>4</sub> molecule. The close analogy between **1** and P<sub>4</sub> is also evident from DFT calculations, which reveal their isolobal electronic structure. The cluster-type core of **1** shows spherical aromaticity. The calculated magnetically induced ring currents are between that of P<sub>4</sub> and the tetrahedrane (*t*BuC)<sub>4</sub> in magnitude and significantly greater than those in benzene. Diphosphate-tetrahdrane **1** is fairly stable in solution in the dark at ambient temperature, while it converts to the ladderane (*t*BuCP)<sub>4</sub> (**2**) upon irradiation or at elevated temperatures. Under UV irradiation, **2** decomposes to P<sub>4</sub> (which, in turn, is transformed into red phosphorus) and di-*tert*-butylacetylene. Based on the NMR and UV/vis spectroscopic monitoring of the photochemical

isomerisation of **1** forming **2** together with quantum chemical calculations, a stepwise mechanism for this reaction is proposed: first, photoexcited **1** isomerises to its 1,2-diphosphacyclobutadiene isomer **1'**, which forms in the excited state on a ps time scale according to molecular dynamics simulations. Subsequently,  $[2 + 2]$  cycloaddition of two 1,2-diphosphacyclobutadienes forms the *endo*-isomer **2-endo** in a purely thermal step without any significant activation barrier. The *endo*-isomer is then photochemically converted into the *exo*-isomer, either directly or by a photochemically induced retro- $[2 + 2]$ -reaction *via* **1'**. The proposed diphosphacyclobutadiene **1'** was trapped as a  $[2 + 2]$  cycloaddition product with *N*-methylmaleimide. The photochemical isomerisation appears to be an intrinsic feature of the reactivity of diphosphatetrahdranes, resulting in diphosphacyclobutadienes as transient intermediates. It is anticipated that this process can be exploited for the generation of various other bi- and tricyclic organophosphorus compounds by reaction with a broader scope of alkenes, alkynes and other unsaturated organic compounds. Such reactions could give rise to a range of new phosphorus heterocycles with interesting properties.

## Data availability

The data supporting the findings of this study are available within the paper and its ESI files.† Raw data are provided on reasonable request. Crystallographic have been deposited at the CCDC under 2102564 and 2323059.

## Author contributions

Gabriele Hierlmeier: conceptualisation, investigation – synthesis and characterisation, writing – original draft. Roger Jan Kutta: investigation – spectroscopy and quantum chemical calculations, writing – original draft. Peter Coburger: investigation – quantum chemical calculations. Hans-Georg Stammer: investigation – X-ray structure analysis of **1**, writing – original draft. Jan Schwabedissen: investigation – X-ray structure analysis of **1**. Norbert W. Mitzel: supervision, writing – review & editing, funding acquisition. Maria Dimitrova: investigation – quantum chemical calculations. Raphael J. F. Berger: investigation – quantum chemical calculations, writing – original draft. Patrick Nuernberger: supervision, writing – review & editing, funding acquisition. Robert Wolf: conceptualization, supervision, writing – review & editing, funding acquisition.

## Conflicts of interest

There are no conflicts to declare.

## Acknowledgements

We thank Verena Streitferdt for the acquisition of initial kinetic data. Financial support by the Deutsche Forschungsgemeinschaft (grant numbers WO1496/10-1 and Mi477/41-1; project numbers 451444676 and 434445823, as well as TRR 325, projects A4 and A5, 444632635) and the Fonds der Chemischen Industrie (Kekulé fellowship for G. H.) is gratefully acknowledged.

## Notes and references

- 1 G. Maier, S. Pfriem, U. Schäfer and R. Matusch, *Angew Chem. Int. Ed. Engl.*, 1978, **17**, 520–521.
- 2 B. M. Cossairt, C. C. Cummins, A. R. Head, D. L. Lichtenberger, R. J. F. Berger, S. A. Hayes, N. W. Mitzel and G. Wu, *J. Am. Chem. Soc.*, 2010, **132**, 8459–8465.
- 3 R. Jupp and J. C. Slootweg, *Angew. Chem., Int. Ed.*, 2020, **59**, 10698–10700.
- 4 Selected review articles: (a) B. M. Cossairt, N. A. Piro and C. C. Cummins, *Chem. Rev.*, 2010, **110**, 4164–4177; (b) M. Caporali, L. Gonsalvi, A. Rossin and M. Peruzzini, *Chem. Rev.*, 2010, **110**, 4178–4235; (c) M. Scheer, G. Balázs and A. Seitz, *Chem. Rev.*, 2010, **110**, 4236–4256; (d) G. Maier, *Angew Chem. Int. Ed. Engl.*, 1988, **27**, 309–332.
- 5 (a) A. Pedler, *J. Chem. Soc., Trans.*, 1890, **57**, 599–613; (b) M. Serrano-Ruiz, A. Romerosa and P. Lorenzo-Luis, *Eur. J. Inorg. Chem.*, 2014, 1587–1598.
- 6 G. Rathenau, *Physica*, 1937, **4**, 503–514.
- 7 (a) O. J. Scherer, *Angew. Chem., Int. Ed.*, 2000, **39**, 1029–1030; (b) H. Bock and H. Mueller, *Inorg. Chem.*, 1984, **23**, 4365–4368; (c) N. A. Piro, J. S. Figueroa, J. T. McKellar and C. C. Cummins, *Science*, 2006, **313**, 1276–1279.
- 8 N. P. Tarasova, Y. V. Smetannikov, I. M. Artemkina, I. A. Lavrov, M. A. Sinaiskii and V. I. Ermakov, *Dokl. Chem.*, 2006, **410**, 189–191.
- 9 (a) D. Tofan and C. C. Cummins, *Angew. Chem., Int. Ed.*, 2010, **49**, 7516–7518; (b) L.-P. Wang, D. Tofan, J. Chen, T. van Voorhis and C. C. Cummins, *RSC Adv.*, 2013, **3**, 23166.
- 10 G. Hierlmeier, P. Coburger, M. Bodensteiner and R. Wolf, *Angew. Chem., Int. Ed.*, 2019, **58**, 16918–16922.
- 11 For reactivity studies on di-*tert*-butyldiphosphatetrahedrane see: (a) G. Hierlmeier, M. K. Uttendorfer and R. Wolf, *Chem. Commun.*, 2021, **57**, 2356–2359; (b) G. Hierlmeier and R. Wolf, *Angew. Chem., Int. Ed.*, 2021, **60**, 6435–6440; (c) G. Hierlmeier, P. Coburger, D. J. Scott, T. M. Maier, S. Pelties, R. Wolf, D. M. Pividori, K. Meyer, N. P. van Leest and B. de Bruin, *Chem.–Eur. J.*, 2021, **27**, 14936–14946; (d) M. K. Uttendorfer, G. Hierlmeier and R. Wolf, *Z. Anorg. Allg. Chem.*, 2022, e202200124.
- 12 (a) M.-L. Y. Riu, R. L. Jones, W. J. Transue, P. Müller and C. C. Cummins, *Sci. Adv.*, 2020, **6**, eaaz3168; (b) M.-L. Y. Riu, M. Ye and C. C. Cummins, *J. Am. Chem. Soc.*, 2021, **143**, 16354–16357.
- 13 S. Geissler, U. Barth, U. Bergsträsser, M. Slany, J. Durkin, P. B. Hitchcock, M. Hofmann, P. Binger, J. F. Nixon, P. von Ragué Schleyer and M. Regitz, *Angew Chem. Int. Ed. Engl.*, 1995, **34**, 484–487.
- 14 M.-L. Y. Riu, A. K. Eckhardt and C. C. Cummins, *J. Am. Chem. Soc.*, 2021, **143**, 13005–13009.
- 15 R. Boese, D. Bläser, R. Latz and A. Bäumen, *Acta Crystallogr.*, 1999, **C55**, IUC9900016.
- 16 H. Inrgartinger, A. Goldmann, R. Jahn, M. Nixdorf, H. Rodewald, G. Maier, K.-D. Malsch and R. Emrich, *Angew Chem. Int. Ed. Engl.*, 1984, **23**, 993–994.
- 17 M. Elian, M. M. L. Chen, D. M. P. Mingos and R. Hoffmann, *Inorg. Chem.*, 1976, **15**, 1148–1155.
- 18 (a) A. Hirsch, Z. Chen and H. Jiao, *Angew. Chem., Int. Ed.*, 2001, **40**, 2834–2838; (b) N. K. V. Monteiro, J. F. de Oliveira and C. L. Firme, *New J. Chem.*, 2014, **38**, 5892–5904; (c) D. Moran, M. Manoharan, T. Heine and P. von Ragué Schleyer, *Org. Lett.*, 2003, **5**, 23–26.
- 19 P. von Ragué Schleyer, C. Maerker, A. Dransfeld, H. Jiao and N. J. R. van Eikema Hommes, *J. Am. Chem. Soc.*, 1996, **118**, 6317–6318.
- 20 P. Weis, D. C. Röhner, R. Prediger, B. Butschke, H. Scherer, S. Weber and I. Krossing, *Chem. Sci.*, 2019, **48**, 295.
- 21 The NICS value of P<sub>4</sub> was also calculated by Cummins (–59.4), see: B. M. Cossairt and C. C. Cummins, *J. Am. Chem. Soc.*, 2009, **131**, 15501–15511.
- 22 D. Sundholm, H. Fliegl and R. J. F. Berger, *Wiley Interdiscip. Rev.: Comput. Mol. Sci.*, 2016, **6**, 639–678.
- 23 It is noteworthy that a significant fraction of the total current density in (tBuC)<sub>4</sub> (about 50% of the diamagnetic contribution) extends over the tBu groups. However, at this stage no further attempts have been made to analyse this phenomenon in more detail.
- 24 K. M. Nicholas and R. Pettit, *Tetrahedron Lett.*, 1971, **12**, 3475–3478.
- 25 Alternatively, it was hypothesised that the intermediate observed at dilute concentration conditions may result from the reaction between 1' and 1 (Fig. S25<sup>†</sup>). According to quantum-chemical calculations, the resulting 'twisted dimer' would represent a stable structure (see the ESI<sup>†</sup> for details). However, its electronic absorption spectrum is expected to show transitions in the visible range from 400 to 500 nm (Fig. S25<sup>†</sup>), which are not observed in any of the experimental data, thus, excluding its formation.
- 26 Intermediate **2-endo** shows considerable stabilisation by dispersion interactions; see: J. P. Wagner and P. R. Schreiner, *Angew. Chem., Int. Ed.*, 2015, **54**, 12274–12296.
- 27 A stepwise bond formation *via* a biradical intermediate is conceivable as an alternative mechanistic pathway for the formation of the *endo*- and *exo*-configured ladderane **2** from 1'. We did not observe such an intermediate, but related biradicals were detected for silicon analogues: J. R. Gee, W. A. Howard, G. L. McPherson and M. J. Fink, *J. Am. Chem. Soc.*, 1991, **113**, 5461–5462.
- 28 We believe that photodimerisation of maleic anhydride is a major competitive pathway, see T. Horie, M. Sumino, T. Tanaka, Y. Matsushita, T. Ichimura and J. Yoshida, *Org. Process Res. Dev.*, 2010, **14**, 405–410.
- 29 (a) B. Cordero, V. Gómez, A. E. Platero-Prats, M. Revés, J. Echeverría, E. Cremades, F. Barragán and S. Alvarez, *Dalton Trans.*, 2008, 2832–2838; (b) P. Pyykkö and M. Atsumi, *Chem.–Eur. J.*, 2009, **15**, 186–197; (c) P. Pyykkö, *J. Phys. Chem. A*, 2015, **119**, 2326–2337.
- 30 W. H. Hersh, S. T. Lam, D. J. Moskovic and A. J. Panagiotakis, *J. Org. Chem.*, 2012, **77**, 4968–4979.
- 31 S. Mack, S. Danner, U. Bergsträsser, H. Heydt and M. Regitz, *J. Organomet. Chem.*, 2002, **643–644**, 409–415.